J Mater Sci (2007) 42:2048–2053
DOI 10.1007/s10853-006-1442-4

# Application of metal injection molding process to fabrication of bulk parts of TiAl intermetallics

**Y. C. Kim · S. Lee · S. Ahn · N. J. Kim**

Received: 6 October 2003 / Accepted: 22 June 2006 / Published online: 28 January 2007


**Abstract** In the present study, a metal injection molding (MIM) process was applied to the fabrication of bulk parts of TiAl intermetallics, and effects of sintering parameters on densification of fabricated parts were investigated. The specimens sintered at 1350 °C showed about the same densification as the ones sintered at 1400 °C, while grains and pores were finer, and thus 1350 °C was chosen as the sintering temperature. In the sintered specimens after debinded in an $H_2$ atmosphere, $Al_2O_3$ precipitates were observed around pores. The densification decreased with increasing heating rate up to the sintering temperature. It was also found that the sintering time increased the densification without grain coarsening. The optimal heating rate was found to be 3 °C/min, and the densification reached a near-full level of 98.8% when sintered at 1350 °C for 30 h. These findings suggested a useful idea to successfully fabricate TiAl intermetallic parts by the MIM process.

Y. C. Kim · S. Ahn
New Materials & Components Research Center/New Metals Research Team, Research Institute of Industrial Science & Technology, Pohang 790-600, Korea

S. Lee (✉) · N. J. Kim
Center for Advanced Aerospace Materials, Pohang University of Science and Technology, Pohang 790-784, Korea
e-mail: shlee@postech.ac.kr

## Introduction

Advanced structural materials used for ultrasonic airplanes or spaceships, high-efficiency gas turbines, and wall structures of nuclear power plants have increasingly required resistance to heat, impact, and environment, specific strength, and specific stiffness. To meet these properties, many new structural materials such as Ti aluminides are under research and development [1, 2]. Particularly, Ti aluminides based on TiAl have been applied to structural and engine parts of airplanes as well as to automobile engine parts because they have low density (~4.5 g/cm$^3$), excellent high-temperature strength and oxidation resistance [3]. However, they have shortcomings such as poor formability because of poor room-temperature ductility and fracture toughness [4, 5].

Recently, a metal injection molding (MIM) process in which net-shape parts are directly fabricated has been developed in order to avoid poor formability of Ti aluminides [6]. In this MIM process, metal powders are mixed with organic binders composed of poly ethylene-ran-vinyl acetate (EVA), paraffin wax, stearic acid, etc., and the mixture undergoes injection molding, debinding, and sintering processes. Since the MIM process can fabricate directly complicated parts of three-dimensional shape in mass production, it may reduce the production cost [7, 8]. However, the size of parts and their continuous production are quite limited because the sintering process should be used in the MIM to minimize pores formed during debinding and to densify them [9–12]. In order to overcome these constraints, studies are highly demanded to delicately control the fabrication process [13–15].

In the present study, the MIM process was newly applied to the fabrication of Ti aluminide parts, and optimal injection molding process variables were obtained. Several injection-molded specimens having different densification were fabricated by varying process parameters, particularly sintering parameters. Pores and phases formed in the MIM process were identified by analyzing microstructures, and their formation mechanisms were investigated.

## Experimental

Powders used for the MIM in this study were Ti–48Al alloy powders fabricated by Sejong Co., Ltd., using self-propagating high-temperature synthesis (SHS) reaction of Ti and Al powders. Impurities of 1.19 wt.% O and 0.05 wt.% C were contained in these powders.

One of important variables in the MIM is to select appropriate binders since they make the mixing and injection molding easier. When they are completely debinded after injection molding, materials having desired properties can be fabricated. Being appropriate binders mean that they should work for homogeneous liquid-phase mixing with metallic powders during the heated mixing process, they should have a good flowability to fill into a mold space with mixed powders during injection molding, and should be readily removed from the molded specimens after injection molding. Since formability and elimination of binders are important considerations, various kinds of wax are widely used as binders. When used alone, waxes are vulnerable to serious expansion and contraction depending on temperature. In this study, poly ethylene-ran-vinyl acetate was mixed with paraffin wax for easier mixing and less volume expansion and with stearic acid for improving the separation from the mold. After dry mixing TiAl powders with binders at 150 °C for 1 h, the mixture was cut into small pieces of 1–5 mm in size, and these powder mixture pieces were loaded in a metal injection machine of 27 ton capacity and then injected into a metallic mold at 120 °C under a pressure of 450 bar.

The process to remove binders from injection molded specimens without causing cracks or defects is called debinding. In the case of TiAl, the debinding process is complicated and takes quite a long time since Al readily forms oxides such as $Al_2O_3$ in reaction with oxygen. In the present study, the debinding process was conducted using both the solvent immersion and the thermal debinding methods. As for the solvent, heptane (normal: $CH_3(CH_2)CH_3$) was used. The 200-mesh sieve, on which the injection molded specimens were placed, was immersed in the solvent, and a stirrer was revolved at 45 °C for 10 h at a speed of 100–150 rpm so that binders were eliminated. When the molded specimens retracted from the solvent were sufficiently dried for 24 h, more than 90% of the binders was removed. To completely eliminate the remaining binders, the specimens were inserted into a tube furnace, kept in an Ar or $H_2$ atmosphere at 300 °C for 1 h, and then at 450 °C for 1 h.

To minimize deformation in the injection molded specimens and to minimize the formation of pores in places where binders were removed due to diffusion, preliminary sintering (pre-sintering) is necessary before sintering. The debinded specimens were inserted into a quartz tube and preliminarily sintered at 1000 °C for 3 h using a tube furnace under a high vacuum of $10^{-5}$ torr. After pre-sintering, the specimens were sintered at 1400 and at 1350 °C, above and below the $\alpha/(\alpha + \gamma)$ transus temperature of the Ti–48Al alloy, respectively. Since the shape and contraction rate of the specimens vary with the heating rate in the tube furnace, the heating rate was varied at 3, 6, and 10 °C/min. The sintering time was also varied in 1, 3, 10, and 30 h in order to investigate the microstructural modification according to sintering time.

Sintered specimens were etched by a Kroll solution (98.5 mL $H_2O$, 1 mL $HNO_3$, 0.5 mL HF), and were observed using an optical microscope and a scanning electron microscope (SEM). Volume fraction of pores present in specimens, i.e., porosity, was measured using an image analyzer. Densification of injection-molded specimens was calculated as 1-porosity. Phases present in Ti–48Al alloy powders and sintered specimens were analyzed by X-ray diffraction (XRD) and energy dispersive spectroscopy (EDS) methods.

## Results and Discussion

An SEM micrograph of TiAl powders is presented in Fig. 1, and shows an irregular shape of TiAl powders sized about 8.7 μm. Density measured using a picnometer is 3.67 g/cm$^3$. Figure 2 is an X-ray diffraction pattern of TiAl powders. A small amount of $\alpha_2$-$Ti_3Al$ phase as well as $\gamma$-TiAl phase is present, together with Ti and Al formed from incomplete SHS reaction.

Figure 3a and b are optical micrographs of the specimens sintered at 1350 and 1400°C for 3 h in a high vacuum without pre-sintering. Densification measured from them is listed in Table 1. The specimen sintered at 1350 °C below the $\alpha/(\alpha + \gamma)$ transus temperature, which is a temperature range where the volume

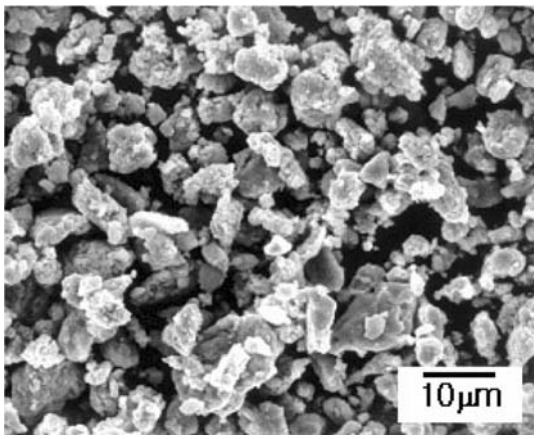


**Fig. 1** SEM micrograph of TiAl powders

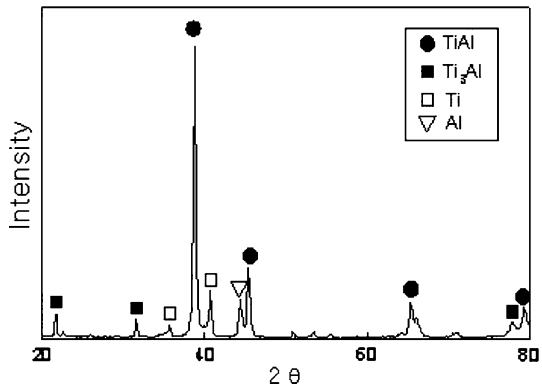


**Fig. 2** X-ray diffraction pattern of TiAl powders, showing peaks of $\gamma$-TiAl, together with small peaks of $\alpha_2$-$Ti_3Al$, Ti, and Al

fraction of $\alpha$ and $\gamma$ is about the same, shows a duplex structure having grains sized about 22 μm (Fig. 3a). The specimen sintered at 1400 °C, above the transus temperature, shows a fully lamellar structure having coarse grains sized about 130 μm (Fig. 3b). In both of the specimens, a considerable amount of pores is observed. Densifications of the specimens sintered at 1350 and 1400 °C are 91.7 and 91.5%, respectively. This indicates that the sintering temperature at around the $\alpha/(\alpha + \gamma)$ transus temperature hardly affects the densification. The sintering at high temperatures is more advantageous in general to raise the densification [16–18], but can deteriorate properties since the high-temperature sintering coarsens grains and enlarges pores [19, 20]. Consequently, 1350 °C was selected as the sintering temperature in this study because grains and pores are finer at 1350 °C than at 1400 °C, while the densification is about the same as at 1400 °C.

Figure 4 is an optical micrograph of the specimen sintered at 1350 °C for 3 h after pre-sintering at 1000 °C for 3 h. It shows increased densification (93.4%) over the specimen of Fig. 3a which was not pre-sintered. This indicates that the pre-sintering is effective to minimize the formation of pores. This specimen was debinded in an Ar atmosphere, which calls for a comparative study with the specimen debinded in an $H_2$ atmosphere to investigate the effect of debinding atmosphere.

An optical micrograph of the specimen pre-sintered at 1000 °C for 3 h and then sintered at 1350 °C for 3 h after being debinded in an $H_2$ atmosphere is shown in Fig. 5a. Here, pores become smaller, and densification significantly rises to 97%. However, unlike in the case of debinding in an Ar atmosphere, fine precipitates sized about 1 μm are observed at grain boundaries as indicated by arrows. These precipitates were analyzed by EDS mapping, and the results are presented in Fig. 5b and c. Since Al and O are detected in the precipitates, they are identified as $Al_2O_3$. This implies that oxides such as $Al_2O_3$ are formed when oxygen in the air is in reaction with Al of TiAl because the specimen is not completely protected from outside air when debinded in the $H_2$ atmosphere, whereas oxides are not formed in the case of debinding in the Ar atmosphere because the protection is complete. $Al_2O_3$ particles are mainly formed around pores where binders are removed during debinding, and are not eliminated after sintering. During sintering, pores are contracted, and their volume fraction is reduced. $Al_2O_3$ particles formed around the pores remain after sintering, and fill in the pores, thereby playing a role to increase the densification. Although $Al_2O_3$ works as an inhibitor to prevent the grain growth during sintering

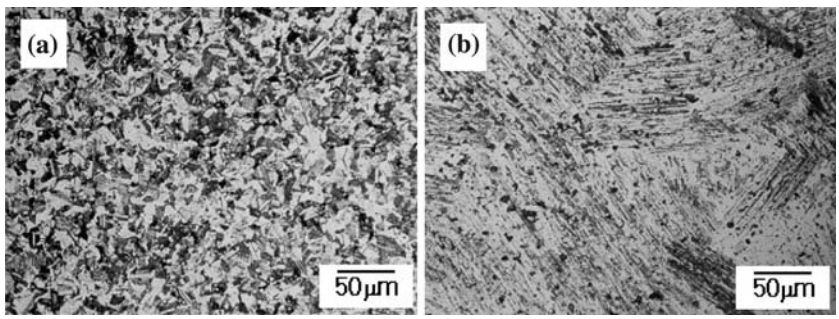


**Fig. 3** Optical micrographs of the specimens sintered at **(a)** 135 °C and **(b)** 1400 °C for 3 h, showing a duplex structure and a fully lamellar structure, respectively. Kroll etched

**Table 1** Quantitative results of densification measured according to the process conditions

| Debinding atmosphere | Pre-sintering condition | Heating rate (°C/min) | Sintering condition | Densification* (%) |
|---|---|---|---|---|
| Ar | – | 3 | 1400 °C, 3 h | 91.5 |
| Ar | – | 3 | 1350 °C, 3 h | 91.7 |
| Ar | 1000 °C, 3 h | 3 | 1350 °C, 3 h | 93.4 |
| $H_2$ | 1000 °C, 3 h | 3 | 1350 °C, 3 h | 97.0 |
| Ar | 1000 °C, 3 h | 6 | 1350 °C, 3 h | 89.7 |
| Ar | 1000 °C, 3 h | 10 | 1350 °C, 3 h | 88.4 |
| Ar | 1000 °C, 3 h | 3 | 1350 °C, 1 h | 91.7 |
| Ar | 1000 °C, 3 h | 3 | 1350 °C, 10 h | 96.0 |
| Ar | 1000 °C, 3 h | 3 | 1350 °C, 30 h | 98.8 |

*Densification = 1 – porosity

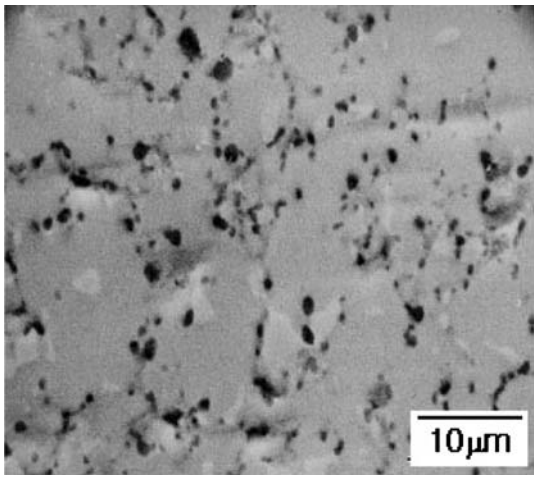


**Fig. 4** Optical micrograph of the specimens sintered at 1350 °C for 3 h after pre-sintering at 1000 °C for 3 h. Not etched

[21, 22], it might be a critical factor seriously deteriorating ductility and fracture toughness because cracks can readily be formed at $Al_2O_3$ and propagated along grain boundaries due to the brittleness of $Al_2O_3$ when a load is applied from outside [23–25]. Therefore, despite increased densification, debinding in an $H_2$ atmosphere is not desirable because of its negative effect on mechanical properties from precipitation of $Al_2O_3$ particles [26, 27].

The heating rate up to the sintering temperature also works as an important variable affecting the shape and volume fraction of pores. Figure 6a–c are SEM micrographs of the specimens sintered at the heating rates of 3, 6, and 10 °C/min. The faster heating rate is accompanied with much higher volume fraction of pores formed at grain boundaries and with larger pores. Table 1 provides the densification of these specimens. At the heating rate of 10 °C/min, the densification is the lowest at 88.4%. This is because,

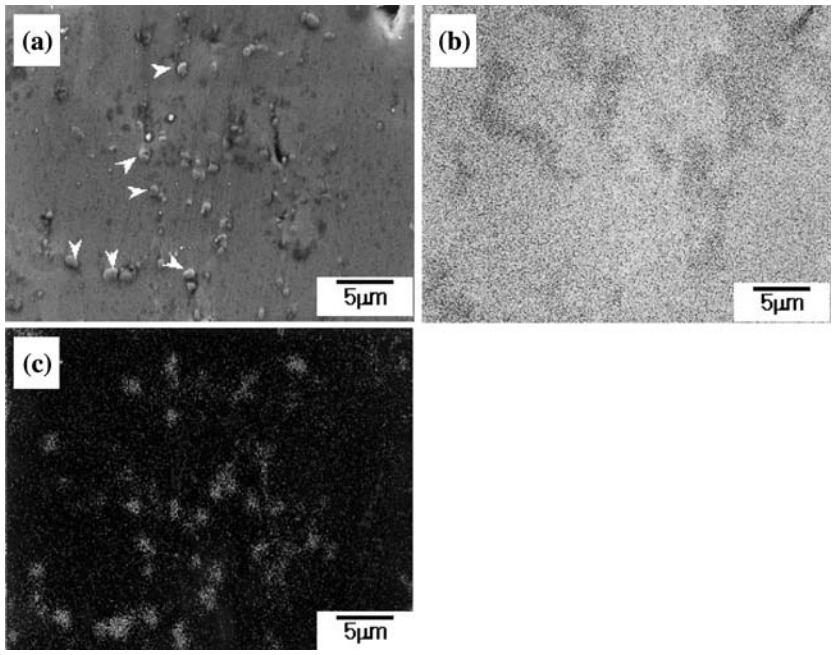


**Fig. 5** **(a)** Optical micrograph of the specimens sintered at 1350 °C for 3 h after debinding at an $H_2$ atmosphere and pre-sintering at 1000 °C for 3 h, showing precipitates at grain boundaries. **(b)** and **(c)** are EDS mapping data of Al and O, respectively, indicating that the grain-boundary precipitates are $Al_2O_3$. Not etched

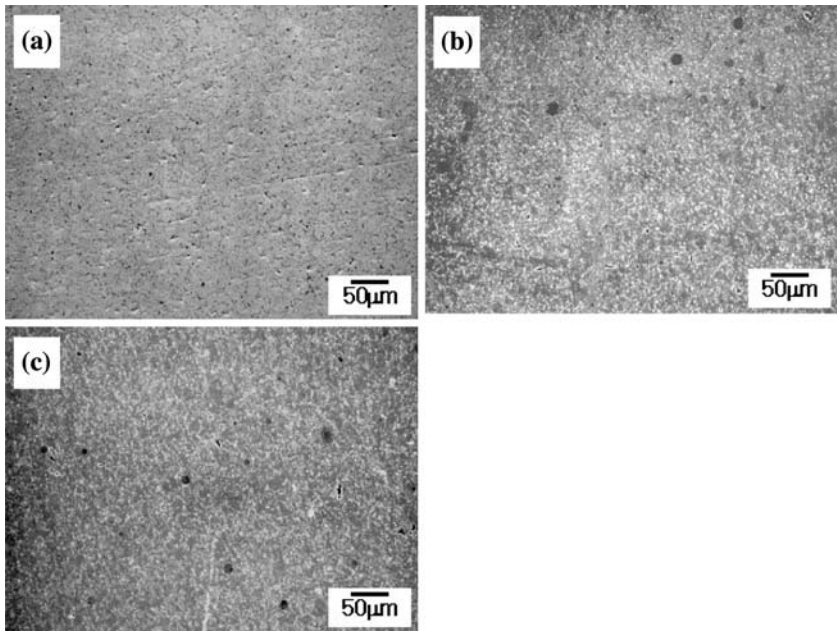


**Fig. 6** SEM micrographs of the specimens sintered with heating rates of **(a)** 3, **(b)** 6, and **(c)** 10 °C /min at 1350 °C for 3 h after pre-sintering at 1000 °C for 3 h. Not etched

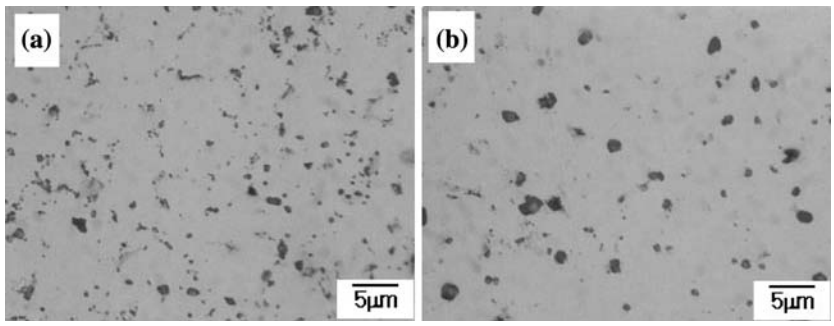


**Fig. 7** SEM micrographs of the specimens sintered at 1350 °C for **(a)** 10 and **(b)** 30 h after pre-sintering at 1000 °C for 3 h. Not etched

at a fast heating rate, the gas generated from remaining binders during sintering or the air inside pores are stuck inside pores due to the lack of time to escape out, and thus pores are not sufficiently contracted. Therefore, the slower heating rates during sintering would be more desirable, but 3 °C /min is more appropriate in consideration of the time consumed for sintering.

Figure 7a and b are optical micrographs of the specimens sintered at 1350 °C for 10 and 30 h after pre-sintering. In comparison with the specimen sintered for 3 h under same conditions (Fig. 4), grains are not coarsened under longer hours of sintering, while the densification is greatly improved, up to 96% in 10-h sintering and further up to 98.8% in 30-h sintering. Particularly, the 30-h sintering, under which the densification is considerably improved without grain coarsening, is the most appropriate condition to obtain highly dense injection molded specimens. It is thus learned that the densification requirement of injection-molded parts can be sufficiently met by controlling the sintering time.

Having newly applied the MIM process in fabricating TiAl parts, this study provides useful data for better understanding of the fabrication process of injection molded TiAl specimens and the mechanism involved in pore formation occurring throughout the injection molding, debinding, and sintering processes. Furthermore, the possibility to fabricate TiAl parts by the MIM process is confirmed in this study. In order to enhance properties of TiAl parts fabricated by the MIM, it is required to select and develop new binders and to investigate the optimal conditions for debinding, pre-sintering, and sintering processes in which densification can be achieved more readily.

## Conclusions

In the present study, concerned with the fabrication of TiAl intermetallic parts using the MIM process, the densification of specimens was studied in terms of the processing variables in injection molding, debinding, and sintering.

(1) The specimens sintered at 1350 °C without pre-sintering showed about the same densification as the ones sintered at 1400 °C, while grains and pores were finer, and thus 1350 °C was chosen as the appropriate sintering temperature in this study. The pre-sintering at 1000 °C for 3 h was effective to minimize the formation of pores.

(2) In the sintered specimens after debinded in an $H_2$ atmosphere, fine $Al_2O_3$ precipitates were observed around pores at grain boundaries. They played a role to fill in the pores and thus increased the densification.

(3) The densification was reduced with increasing heating rate up to the sintering temperature. This was because of the lack of sufficient time for the gas or air generated from remaining binders to escape during sintering. It was also found that longer sintering time was accompanied with higher densification, but without grain coarsening. The optimal heating rate was found to be 3 °C/min, and the densification reached a near-full level of 98.8% when sintered at 1350 °C for 30 h.

## References


1. Chang WS, Muddle BC (1996) Metal Mater 2(4):233
2. Kim MG, Kim YJ (2002) Metal Mater Int 8(3):289
3. Kim YW (1992) Acta Mater 40:1121
4. Hartfield-Wunsch SE, Sperling AA, Morrison RS, Dowling WE, Allison JE (1995) In: Kim YW, Wagner R, Yamaguchi M (eds) Gamma titanium aluminides, TMS. Las Vegas, p 41
5. Kim HY, Hong SH (1998) Metal Mater 4(4):765
6. Chang WS, Muddle BC (1997) Metal Mater 3(1):1
7. Dimiduk DM, Mirade DB (1989) High-temperature ordered intermetallic alloys III, MRS. Pittsburgh, p 349
8. Fleischer RL (1987) High-temperature ordered intermetallic alloys II, MRS. Pittsburgh, p 405
9. Horata A (1997) Metal Power Rep 10:41
10. Kim YJ, Hyun SK, Kim MS (1997) J Kor Power Metall 4:243
11. Kato K, Nozaki Y, Matsumoto A (1992) J Jpn Power Metall 39:875
12. Kato K (1997) Metal Power Rep 9:43
13. Soboyejo WO, Schwartz DS, Sastry SML (1992) Metall Mater Trans 23:2039
14. Boodey JB, Gao M, Wei W, Wei RP (1995) In: Kim YW, Wagner R, Yamaguchi M (eds) Gamma titanium aluminides, TMS. Las Vegas, p 101
15. Nelson HG (1993) In: Stoloff NS, Duquette DJ, Giamei AF (eds) Critical issues in the development of high temperature structural materials, TMS. p 455
16. Mizuno Y, Kawasaki A, Watanabe R (1996) J Jpn Inst Metals 60:106
17. Kovacs K, Perczel IV, Josepovits VK, Kiss G, Reti F, Deak P (2002) Appl Surf Sci 200:185
18. Mei B, Miyamoto Y (2002) Mater Chem Phys 75:291
19. Suga H (1997) Metal Power Rep 9:52
20. Ryu HJ, Hong SH (2001) Metal Mater Int 7(3):221
21. Lee DB (2005) Metal Mater Int 11(2):141
22. Lee DB (2005) Metal Mater Int 11(4):313
23. Fang W, Ko SH, Hashimoto H, Abe T, Park Y.-H (2002) Mater Sci Eng 329–331:708
24. Lee DB, Kim MH, Kim SE, Lee JY, Park KB, Moon JJ, Choi SC, Yang CW (2001) Metal Mater 7:143
25. Kim BG, Kim GM, Kim CJ (1995) Scripta Mater 33:1117
26. Hashi K, Ishikawa K, Aoki K (2001) Metal Mater Int 7(2):175
27. Park KS, Bae DS, Lee GH, Lee SK (2005) Metal Mater Int 11(6):481